CHAPTER 3

Energy Analysis of a Solar-Absorption Heat Transformer Combining with a Vapor Compression Heat Pump

This chapter presents simulation results of a H_2O-LiBr absorption heat transformer (AHT) performance having a vapor compression heat pump (VCHP) recovering heat at the AHT condenser which is transferred to the AHT evaporator. The unit of 10 kW_{th} AHT is used to upgrade heat from a solar hot water heater of which the heat is supplied by a set of flat-plate solar collectors each in parallel connection. The weather and the solar radiation data of Chiang Mai, Thailand are the input information for the calculation.

3.1 Introduction

In tropical area, even solar radiation level is rather high but diffuse solar radiation component is also very significant thus only flat-pate solar collector could be competitive with conventional energy for heat generation. Normally, the flat-plate one could not supply heat with a temperature over 70 $^{\circ}C$, otherwise its thermal efficiency is very low then a technique to boost-up the temperature is needed.

In a conventional absorption heat transformer (AHT), low temperature heat is absorbed at the AHT generator and the AHT evaporator while high temperature heat is delivered at the AHT absorber and there is waste heat rejected at the AHT condenser. Studies on energy analyses of the AHT have been reported by various literatures. Sozen (2003) reported performance of an AHT that was used to increase a solar pond's temperature. The coefficient of performance (COP) and the maximum temperature were around 0.4 and 150 $^{\circ}C$, respectively. Sencan et al. (2005) presented performance analysis of a H_2O-LiBr absorption system. It could be seen that the cooling and heating COPs of the system increased slightly when increasing the heat source temperature. Rivara et al. (2009) reported energy analysis of a single-stage H_2O-LiBr AHT of which the highest COP was obtained at the highest solution concentration at around 0.4.

Normally, the overall COP of the H_2O-LiBr AHT could not be over 0.5. Therefore, the heat rejected at the AHT condenser could be recovered and supplied back to the AHT evaporator then the COP could be increased. Therefore, in this study a method to improve thermal performance of a single-stage H_2O-LiBr AHT by combining a VCHP to recover and supply the heat rejected from the AHT condenser back to the AHT evaporator is considered.

In this study an AHT coupling with a VCHP is used to upgrade solar heat from flat-plate solar collectors. With this approach, input heat form solar collectors could be supplied at the AHT generator only, thus the number of the solar collectors could be reduced.

3.2 System Description

Figure 3.1 shows a schematic sketch of a general solar-absorption heat transformer (Solar-AHT). Solar heat is supplied to the AHT generator and the AHT evaporator at a medium temperature (around 60-80 $^{\circ}$C) and rejected heat at a lower temperature (around 35-45 $^{\circ}$C) at the AHT condenser. The upgrading heat at a higher temperature (around 90-110 $^{\circ}$C) is obtained at the AHT absorber. At the AHT condenser, high amount of heat rate is rejected to the environment thus the coefficient of performance (COP) of the normal AHT system is rather low. Moreover, high number of the solar collectors for generating hot water at the AHT generator and the evaporator is needed which results in high investment cost and the payback period is rather long.

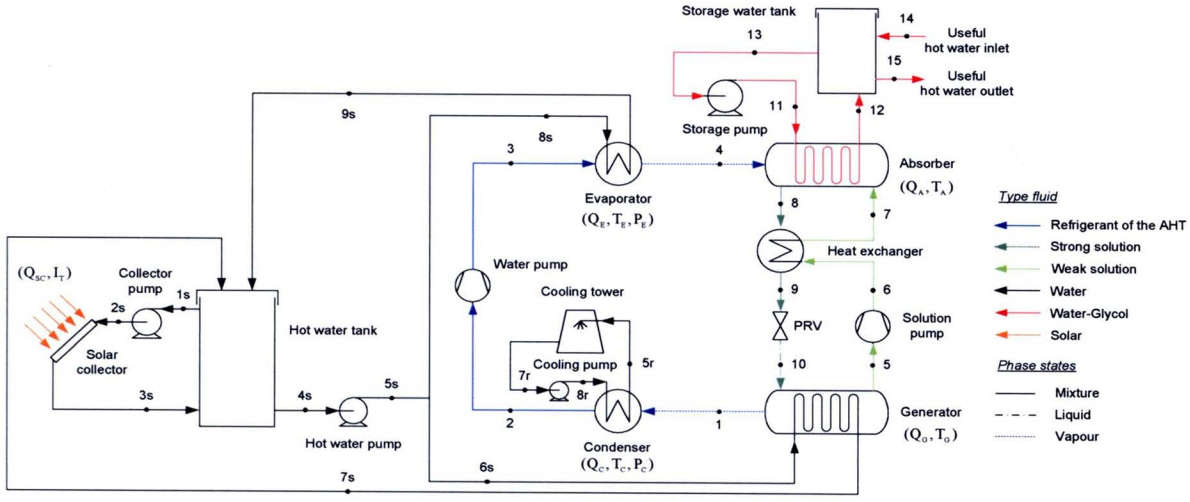

Figure 3.1 Schematic diagram of a solar-absorption heat transformer.

In this study, an AHT coupling with a VCHP namely compression/absorption heat transformer (CAHT) is considered. The heat rejected at the AHT condenser is recovered by a single-stage VCHP then the heat is upgraded and generated back to the AHT evaporator. Besides, the solar collector will supply only at the AHT generator then the number of solar collectors could be less and the overall COP could be increased since there is no heat loss at the AHT condenser. Figure 3.2 shows a schematic diagram of the CAHT. R-123 is selected as the working fluid of the single-stage VCHP.

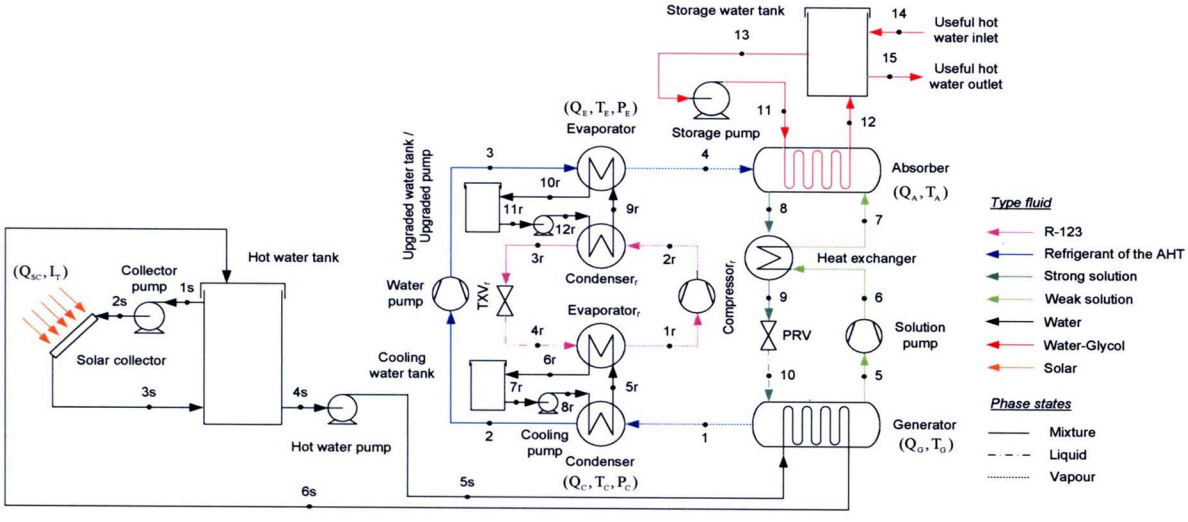

Figure 3.2 Schematic diagram of a solar-AHT coupling with a single-stage VCHP.

3.3 System Simulation

3.3.1 Solar Water Heating System

In the calculation, the heat transfer rate from the solar collector (Q_{sc}) is calculated as follows:

- Solar radiation

The time used in the calculation is the solar time which could be calculated from the standard time and the longitude (Duffie and Beckman, 1980) as

$$\text{Solar time - Standard time} = 4(L_{Std} - L_{Loc}) + E, \tag{3.1}$$

when

$$E = 9.87\sin(2B) - 7.53\cos B - 1.5\sin B, \tag{3.2}$$

$$B = \frac{360(n-1)}{365}. \tag{3.3}$$

The total daily extraterrestrial radiation on a horizontal surface over a day (H_o) could be calculated by

$$H_o = \frac{24\times 3600}{\pi} G_{sc}\left[1 + 0.033\cos\left(\frac{360n}{365}\right)\right]\times\left[\cos\varphi\cos\delta\sin\omega_s + \frac{2\pi\omega_s}{360}\sin\varphi\sin\delta\right], \tag{3.4}$$

when

$$\delta = 23.45\sin\left[\frac{360(284+n)}{365}\right], \tag{3.5}$$

$$\omega_s = \cos^{-1}\left[\frac{\sin\varphi\sin\delta}{\cos\varphi\cos\delta}\right] = \cos^{-1}(-\tan\varphi\tan\delta). \tag{3.6}$$

The daily diffuse solar radiation (H_d) for Thailand (Wongratanaphisan et al., 2003) could be calculated from the global solar radiation, H, and H_o as

$$\frac{H_d}{H_o} = -4.6408 + 26.5495\left(\frac{H}{H_o}\right) - 28.3422\left(\frac{H}{H_o}\right)^2 - 31.4546\left(\frac{H}{H_o}\right)^3 + 46.4421\left(\frac{H}{H_o}\right)^4. \tag{3.7}$$

Then the direct radiation H_b could be calculated from

$$H = H_b + H_d. \tag{3.8}$$

For the simulation, the calculation is performed by taking the representative day of each month. Table 3.1 shows the representative days for all months (Duffie and Beckman, 1980).

Table 3.1 Julian date of each month (Duffie and Beckman, 1980).

Month	Jan	Feb	Mar	Apr	May	Jun	Jul	Aug	Sep	Oct	Nov	Dec
Date of month	17	16	16	15	15	11	17	16	15	15	14	10
Julian date (n)	17	47	75	105	135	162	198	228	258	288	318	344

The hourly solar radiation could be calculated as follows:

For hourly solar radiation (I),

$$\frac{I}{H}=\frac{\pi}{24}\times\frac{(a+b\cos\omega)(\cos\omega-\cos\omega_s)}{\sin\omega_s-\frac{2\pi\omega_s\cos\omega_s}{360}}, \tag{3.9}$$

where

$$a=a_1+a_2\sin(\omega_s-60^\circ), \tag{3.10}$$

$$b=b_1+b_2\sin(\omega_s-60^\circ). \tag{3.11}$$

The constants a_1, a_2, b_1, b_2 for Thailand are shown in Table 3.2.

Table 3.2 The constant of a_1, a_2, b_1 and b_2 for some main provinces in Thailand (Wongratanaphisan et al., 2003).

Province	a_1	a_2	b_1	b_2
Chiang Mai	0.514	0.228	0.512	0.033
Ubon Ratchathani	0.760	– 0.031	0.207	0.238
Had Yai	0.307	– 0.124	0.417	0.007
Bangkok	0.792	– 0.250	0.189	0.471

For hourly diffuse solar radiation (I_d),

$$\frac{I_d}{H_d}=\frac{\pi}{24}\times\frac{\cos\omega-\cos\omega_s}{\sin\omega_s-\frac{2\pi\omega_s\cos\omega_s}{360}}. \tag{3.12}$$

Then the hourly direct solar radiation (I_b) could be calculated from

$$I_b = I - I_d . \tag{3.13}$$

The hourly solar radiation on an inclined plane (I_t) could be calculated from

$$I_t = I_b R_b + I_d \frac{1+\cos\beta}{2} . \tag{3.14}$$

When there is an effect on the floor albedo, the equation becomes

$$I_t = I_b R_b + I_d \frac{1+\cos\beta}{2} + \rho_g (I_b + I_d)\left(\frac{1-\cos\beta}{2}\right). \tag{3.15}$$

R_b is calculated by

$$R_b = \frac{\cos\theta}{\cos\theta_z}, \tag{3.16}$$

where

$$\cos\theta = \sin\delta\sin\varphi\cos\beta - \sin\delta\cos\varphi\sin\beta\cos\gamma + \cos\delta\cos\varphi\cos\beta\cos\omega + \cos\delta\sin\varphi\sin\beta\cos\gamma\cos\omega + \cos\delta\sin\beta\sin\gamma\sin\omega , \tag{3.17}$$

$$\cos\theta_z = \sin\delta\sin\varphi + \cos\delta\cos\varphi\cos\omega . \tag{3.18}$$

- Solar collector

$$Q_{SC} = \dot{m}_{SC} Cp_{SC} (T_{SC,o} - T_{SC,i}) , \tag{3.19}$$

$$Q_{SC} = F_R (\tau\alpha) I_t A_{SC} - F_R U_L A_{SC} (T_{SC,i} - T_a) . \tag{3.20}$$

For solar collectors in series connection (Duffie and Beckman, 1980)

$$(F_R(\tau\alpha))_{Series} = F_R(\tau\alpha)\left[\frac{1-(1-K)^N}{NK}\right], \tag{3.21}$$

$$(F_R U_L)_{Series} = F_R U_L \left[\frac{1-(1-K)^N}{NK}\right] . \tag{3.22}$$

Where

$$K = \frac{A_{SC}(F_R U_L)_{Single\ unit}}{\dot{m}_{SC} Cp_{SC}} . \tag{3.23}$$

- Supplied heat rate at storage tank

$$Q_{Sup} = \dot{m}_{Sup} Cp_{bulk} (T_{Sup,o} - T_{Sup,i}) . \tag{3.24}$$

- Heat loss at storage tank

$$Q_{Loss} = UA_{Tank}(T_{1s} - T_a) . \quad (3.25)$$

- Storage tank

$$Q_{ST} = M_{ST} Cp_{ST} \left(\frac{T_{ST}^{t+\Delta t} - T_{ST}^{t}}{\Delta t}\right) . \quad (3.26)$$

Using numerical method, the water temperature could be calculated from,

$$T_{ST}^{t+\Delta t} = T_{ST}^{t} + \frac{Q_{ST}\Delta t}{M_{ST} Cp_{ST}} . \quad (3.27)$$

When an auxiliary heat is included, the equation could be rewritten as

$$T_{ST}^{t+\Delta t} = T_{ST}^{t} + \frac{(Q_{SC} + Q_{Aux} - Q_{loss} - Q_{Sup})\Delta t}{M_{ST} Cp_{ST}} . \quad (3.28)$$

T_{ST}^{t} is the water temperature at time t and $T_{ST}^{t+\Delta t}$ is the value after the time lapse Δt.

Figure 3.3 shows calculation steps for evaluating a normal solar water heating system. The calculation process of the solar radiation is started to evaluate the hourly solar radiation (I_t), then, this value is the input data for calculating thermal performance of the solar water heating system. The output of this part is the hot water temperature in the storage tank.

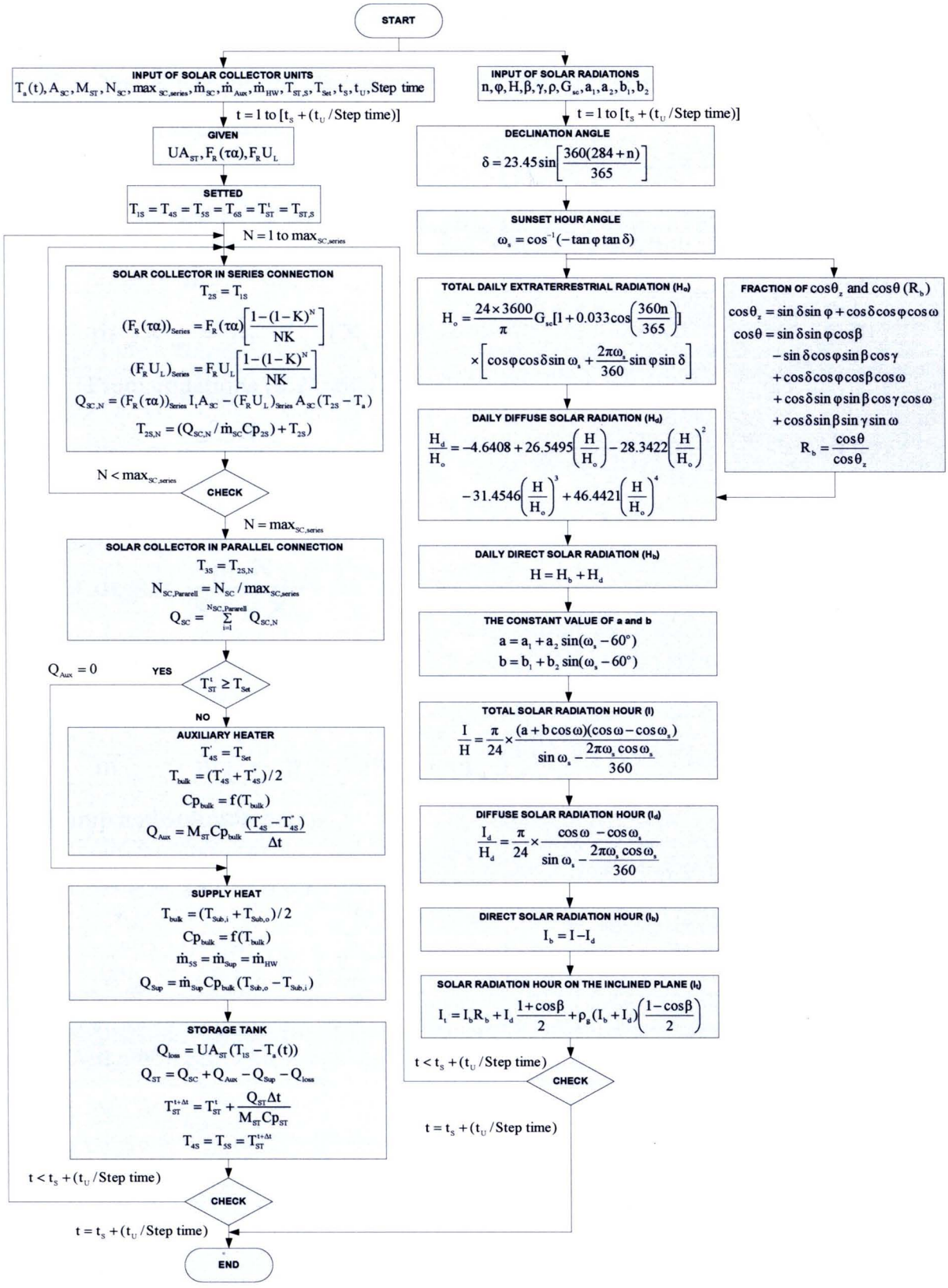

Figure 3.3 Calculation steps for evaluating performance of the solar water heating system.

3.3.2 Absorption Heat Transformer

The equations for all components in the AHT cycle given in Figure 3.1 and Figure 3.2 are as follows:

- Generator

$$Q_G = \dot{m}_1 h_1 + \dot{m}_5 h_5 - \dot{m}_{10} h_{10}, \tag{3.29}$$

$$\dot{m}_{10} = \dot{m}_1 + \dot{m}_5, \tag{3.30}$$

$$\dot{m}_{10} X_{10} = \dot{m}_5 X_5, (X_1 = 0). \tag{3.31}$$

From equations (2.2) and (2.3)

$$\dot{m}_5 = \frac{\dot{m}_1 X_{10}}{X_5 - X_{10}}, \tag{3.32}$$

and

$$\dot{m}_{10} = \frac{\dot{m}_1 X_5}{X_5 - X_{10}}. \tag{3.33}$$

- Condenser

$$Q_C = \dot{m}_{ref} (h_1 - h_2), \tag{3.34}$$

$$\dot{m}_{ref} = \dot{m}_1 = \dot{m}_2 = \dot{m}_3 = \dot{m}_4. \tag{3.35}$$

- Pump and solution pump

$$W_P = (P_E - P_C) \frac{v_2 \dot{m}_2}{\eta_P}, \tag{3.36}$$

$$W_{SP} = (P_E - P_C) \frac{v_5 \dot{m}_5}{\eta_{SP}}, \tag{3.37}$$

$$h_2 \approx h_3, \tag{3.38}$$

$$h_5 \approx h_6. \tag{3.39}$$

- Evaporator

$$Q_E = \dot{m}_{ref} (h_4 - h_3). \tag{3.40}$$

- Absorber

$$Q_A = \dot{m}_4 h_4 + \dot{m}_7 h_7 - \dot{m}_8 h_8, \tag{3.41}$$

$$\dot{m}_8 = \dot{m}_4 + \dot{m}_7 , \tag{3.42}$$

$$\dot{m}_8 X_8 = \dot{m}_7 X_7 . \tag{3.43}$$

- Heat exchanger

$$Q_{HX} = \dot{m}_8 Cp_8 (T_8 - T_9) = \dot{m}_6 Cp_6 (T_7 - T_6) = \varepsilon_{HX} (mCp)_{min} (T_8 - T_6) , \tag{3.44}$$

$$\dot{m}_8 = \dot{m}_9 , \tag{3.45}$$

$$\dot{m}_6 = \dot{m}_7 . \tag{3.46}$$

- Expansion valve

$$h_9 = h_{10} \text{ (Throttling process).} \tag{3.47}$$

- Flow ratio (FR)

$$FR = \frac{\dot{m}_5}{\dot{m}_{ref}} . \tag{3.48}$$

- Coefficient of performance (COP)

$$COP_{AHT} = \frac{Q_A}{Q_E + Q_G + W_P + W_{SP}} . \tag{3.49}$$

3.3.3 Vapor Compression Heat Pump Cycle

a. Single-Stage Cycle

Figure 3.2 shows a schematic diagram of an AHT coupling with a single-stage vapor compression heat pump (CAHT). The heat rejected at the AHT condenser is recovered by the VCHP then upgraded and supplied to the AHT evaporator.

The basic equations for the behavior of each component in the VCHP cycle as presented in Figure 3.2 are as follows:

- Evaporator$_r$

$$Q_{Er} = \dot{m}_r (h_{1r} - h_{4r}) , \tag{3.50}$$

$$\dot{m}_r = \dot{m}_{1r} = \dot{m}_{2r} = \dot{m}_{3r} = \dot{m}_{4r} . \tag{3.51}$$

- Compressor$_r$

$$W_{Comp} = \dot{m}_r (h_{2r} - h_{1r}) , \tag{3.52}$$

$$s_{1r} = s_{2r} \text{ (Isentropic process),} \tag{3.53}$$

$$\eta_{Comp} = \frac{h'_{2r} - h_{1r}}{h_{2r} - h_{1r}}. \tag{3.54}$$

- Condenser$_r$

$$Q_{Cr} = \dot{m}_r (h_{2r} - h_{3r}). \tag{3.55}$$

- Expansion valve$_r$

$$h_{3r} = h_{4r} \text{ (Throttling process).} \tag{3.56}$$

- Coefficient of performance (COP)

$$COP_{VCHP} = \frac{Q_{Cr}}{W_{Comp}}. \tag{3.57}$$

R-123 is selected as the working fluid of the VCHP due to its low compression work at a high temperature range and the cycle pressure ratio is not high.

b. Two-Stage Cycles

In this study, a two-stage VCHP to recover the waste hest is also considered. Figure 3.4 shows the diagram of the CAHT with the two-stage VCHP. The working fluids for the low pressure and the high pressure cycles are R134a and R123, respectively. The energy equations at all the components are as follows:

- Evaporator$_r$

$$Q_{Er} = \dot{m}_{r1} (h_{1r} - h_{4r}), \tag{3.58}$$

$$\dot{m}_{r1} = \dot{m}_{1r} = \dot{m}_{2r} = \dot{m}_{3r} = \dot{m}_{4r}. \tag{3.59}$$

- Economizer$_r$

$$Q_{EC} = \dot{m}_{r2} (h_{5r} - h_{8r}), \tag{3.60}$$

$$\dot{m}_{r2} = \dot{m}_{5r} = \dot{m}_{6r} = \dot{m}_{7r} = \dot{m}_{8r}. \tag{3.61}$$

- Compressor$_r$

$$W_{Comp1} = \dot{m}_{r1} (h_{2r} - h_{1r}), \; W_{Comp2} = \dot{m}_{r2} (h_{2r} - h_{1r}), \tag{3.62}$$

$$s_{1r} = s_{2r}, \; s_{5r} = s_{6r} \text{ (Isentropic process),} \tag{3.63}$$

$$\eta_{Comp1} = \frac{h'_{2r} - h_{1r}}{h_{2r} - h_{1r}}, \; \eta_{Comp2} = \frac{h'_{6r} - h_{5r}}{h_{6r} - h_{5r}}. \tag{3.64}$$

- Condenser$_r$

$$Q_{Cr} = \dot{m}_{r2}(h_{6r} - h_{7r}) . \tag{3.65}$$

- Expansion valve$_r$

$$h_{3r} = h_{4r}\ ,\ h_{7r} = h_{8r}\ \text{(Throttling process)}. \tag{3.66}$$

- Coefficient of performance (COP)

$$COP_{VCHP} = \frac{Q_{Cr}}{W_{Comp}} . \tag{3.67}$$

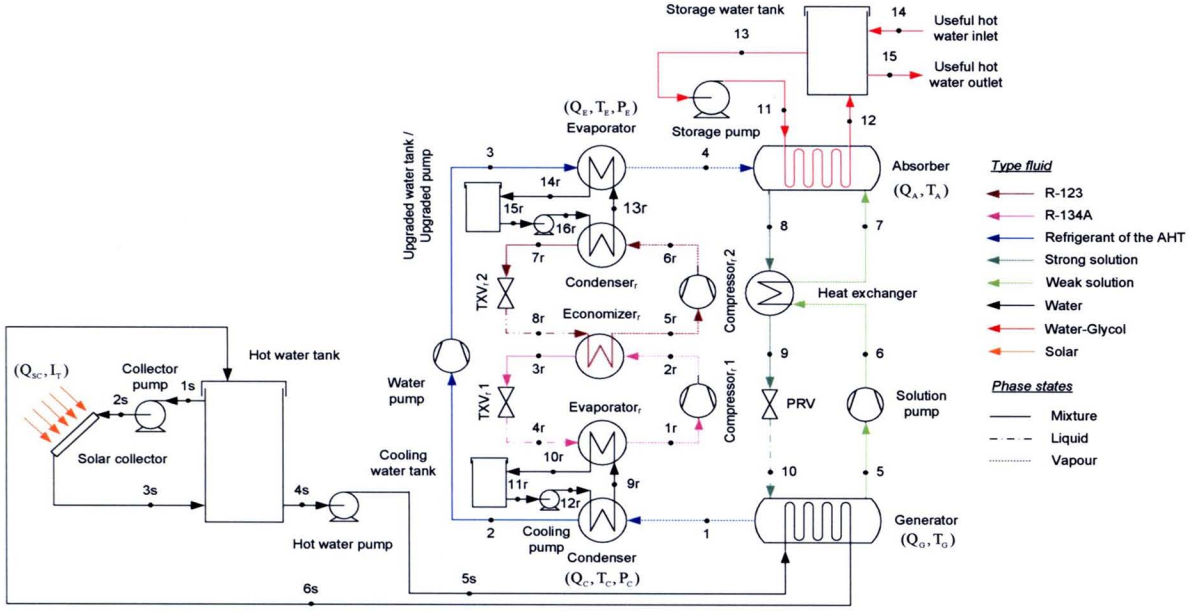

Figure 3.4 Schematic diagram of a solar-AHT coupling with a single-stage VCHP

When the AHT and the CAHT are used to upgrade heat from flat-plate solar collectors, the solar heat is supplied at the evaporator and the generator of the AHT for the previous case and only at the generator for the latter one. The temperature inlet of solar collector is assumed to be 5 °C higher than that of the AHT evaporator and generator. The supplied heat rate could be

For the conventional AHT:

$$Q_E = A_{C,E}[F_R(\tau\alpha)I_T - F_R U_L(T_E + 5 - T_a)\,, \tag{3.68a}$$

For the AHT and the CAHT:

$$Q_G = A_{C,G}[F_R(\tau\alpha)I_T - F_R U_L(T_G + 5 - T_a)\,. \tag{3.68b}$$

The steps for calculating the CAHT performance with the single-stage VCHP and the two-stage VCHP are shown in Figures 3.4 and 3.5, respectively. Input data of the both simulation are supplied hot water of the AHT ($T_{HS,i}$) from the solar water heating system, water flow rate ($\dot{m}_{HS}$) entering the AHT generator and the AHT evaporator each at 0.5 l/s. The working fluids in the single-stage VCHP and the two-stage VCHP are R-123 and R-134A/R-123, respectively. In the calculations, the thermodynamic properties of working fluids of the AHT system and the VCHP system are evaluated to find out the overall COP of both CAHT and AHT systems.

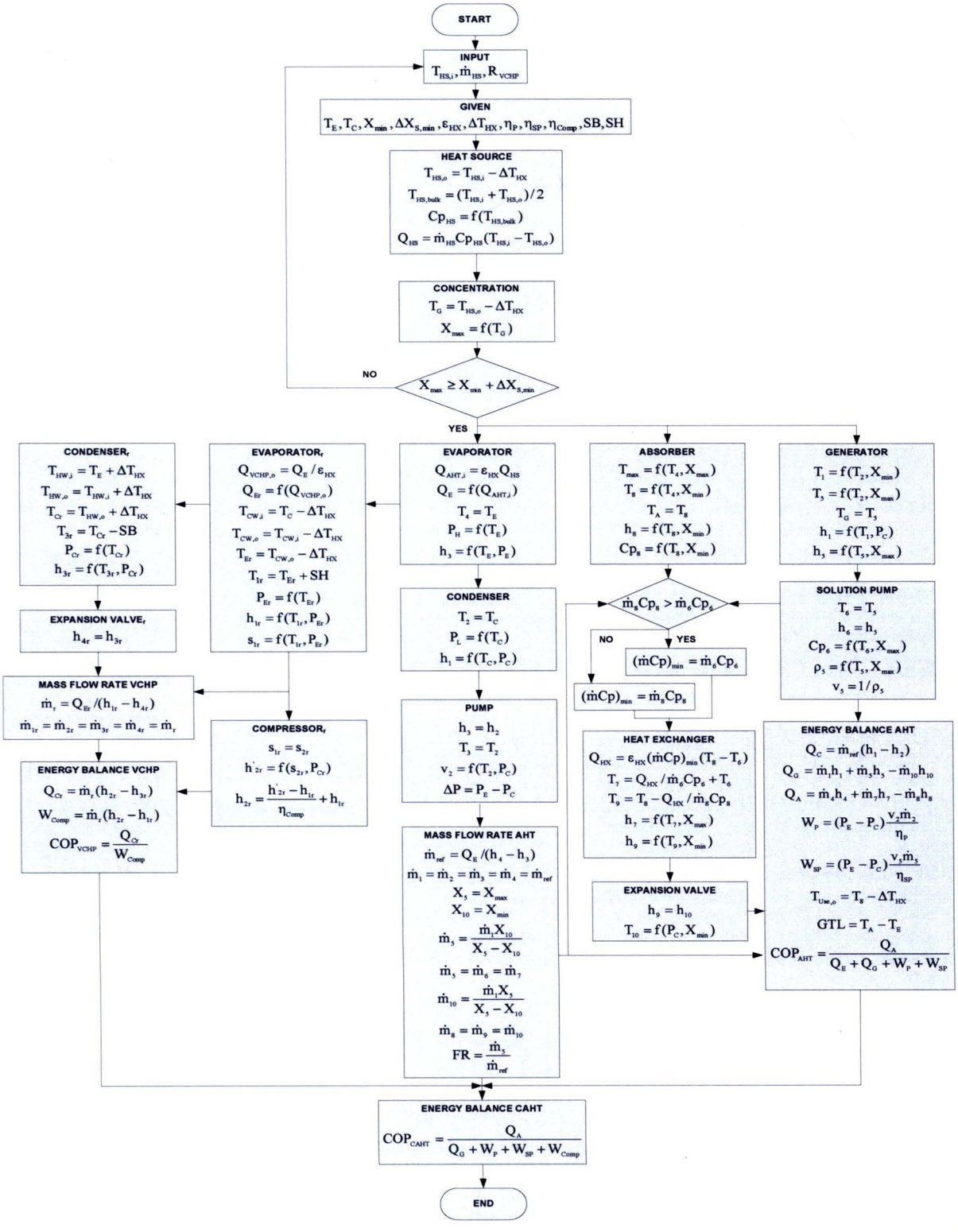

Figure 3.5 Flow chart of the simulation program for evaluating the CAHT performance when a single-stage VCHP is coupled with.

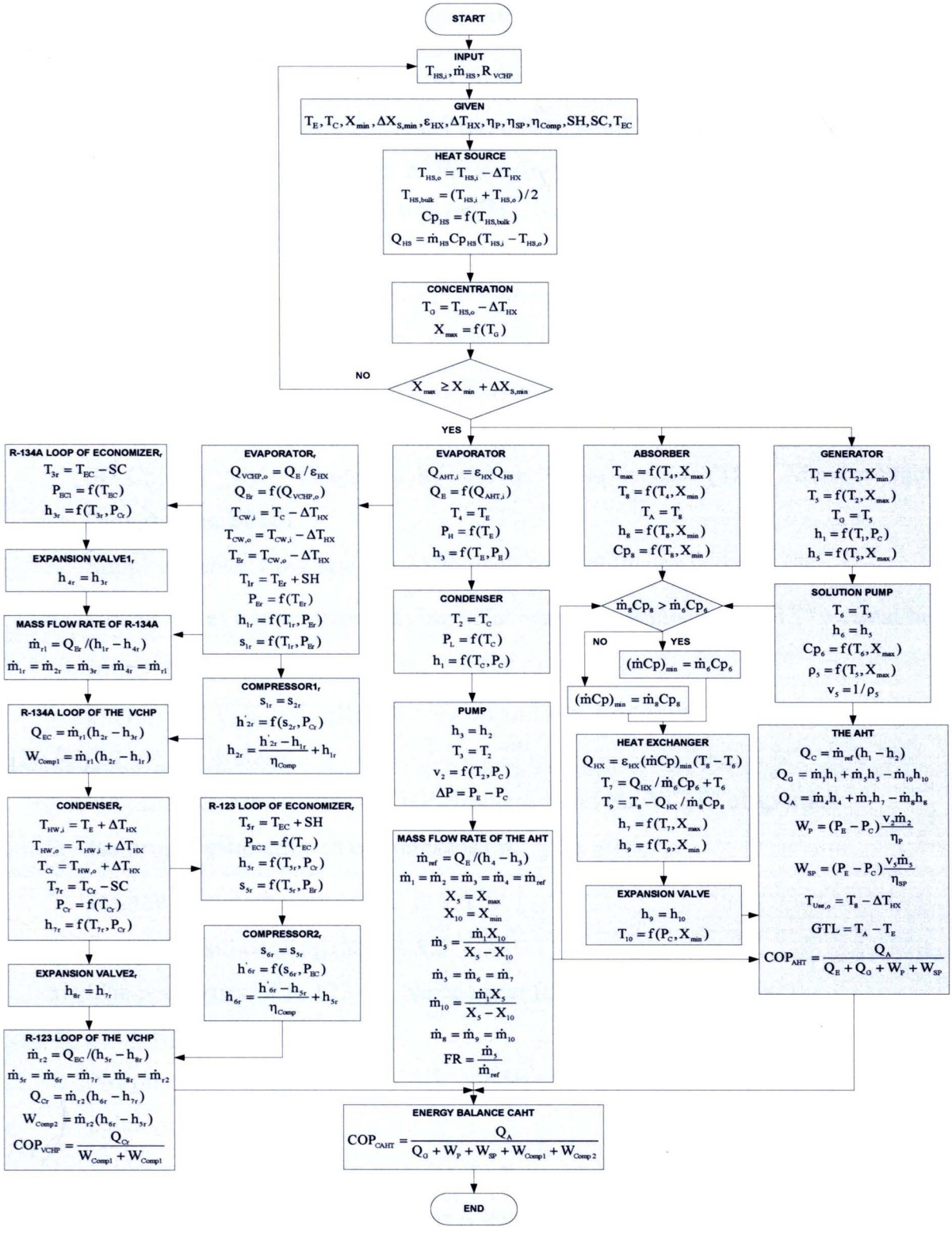

Figure 3.6 Flow chart of the simulation program for evaluating the CAHT combining with the two-stage VCHP performance.

3.4 Operating Conditions and Assumptions

All calculations of the solar-AHT and solar-CAHT are based on the systems presented in Figure 3.1, Figure 3.2 and Figure 3.4. The H_2O-LiBr is the working pair of the AHT, R-123 is the refrigerant of the single-stage VCHP and R-134A and R-123 are the refrigerant of the two-stage VCHP. The working conditions for the evaluation are:

Solar water heating system

1. The solar radiation (I_T) used for the simulation is the mean solar radiation level of Chiang Mai, Thailand, as shown in appendix (RETScreen data, 2010).
2. The ambient temperature (T_a) used for the simulation is the mean temperature of Chiang Mai, Thailand, as shown in appendix (Thai Meteorological Department, 2010).
3. Supplied water flow rate ($\dot{m}_{SC}$) to each solar collector is 0.043 l/s.
4. Useful water temperature leaving solar water heating system ($T_{ST}^{t+\Delta t}$) equal heat source temperature entering the CAHT (T_{5S}).
5. $F_R(\tau\alpha)$ and $F_R U_L$ of collector are constants at 2 m^2/unit.

The R-123 VCHP system

1. No pressure drops at the VCHP condenser and the VCHP evaporator.
2. Isentropic efficiency of compressor (η_{Comp}) is 80%.
3. Degree of superheating (SH) is 5.0 °C.
4. Degree of subcooling (SC) is 5.0 °C.
5. The properties of R-123 are based upon REFPROP (NIST, 2000).

The R-134A/R-123 VCHP system

1. No pressure drops at the VCHP condenser, the VCHP evaporator and VCHP economizer.
2. Isentropic efficiency of compressor (η_{Comp1} and η_{Comp2}) is 80%.
3. Degree of superheating (SH) is 5.0 °C.
4. Degree of subcooling (SC) is 5.0 °C.
5. The temperature at the VCHP economizer (T_{EC}) is 65 °C.
6. The properties of R-134A and R-123 are based upon REFPROP (NIST, 2000).

The AHT system

1. Useful heat leaving the AHT absorber is around 10 kW.
2. Minimum concentration of weak H_2O-LiBr solution (X_{min}) is 45 %LiBr.
3. Maximum flow ratio (FR) for starting is around 20 %LiBr.
4. No pressure drops at the AHT condenser, the AHT generator, the AHT evaporator, the AHT absorber and the AHT heat exchanger.
5. Isentropic efficiencies of water pump (η_P) and solution pump (η_{SP}) are 85%.
6. Effectiveness of the AHT heat exchanger (ε_{HX}) is 85%.
7. Temperature difference between the outlet supplied hot water and the AHT generator is 5 °C.
8. Temperature difference between the outlet useful water and the AHT absorber is 5 °C.
9. Temperature difference between the outlet cooling water and the AHT condenser is 5 °C.
10. Temperature difference between the outlet supplied hot water and the AHT evaporator is 5 °C.
11. The properties of H_2O-LiBr solution are shown in appendix C (ASHRAE, 2001).

3.5 Results and Discussions

3.5.1 Thermal performance of the AHT

For the AHT system, Figure 3.7 shows the temperature profiles of the main component in the AHT system with various values of the supplied hot water temperature. It could be seen that the AHT generator could be started up when the hot water temperature is over about 58 °C and the percentage of LiBr in the salt solution is over 45 %. Thus the appropriate temperature for operating the AHT system if solar collector is taken as a heat generator should be around 60-70 °C. When the water temperature is too high, the solar collector efficiency is reduced and the collectors might not operate.

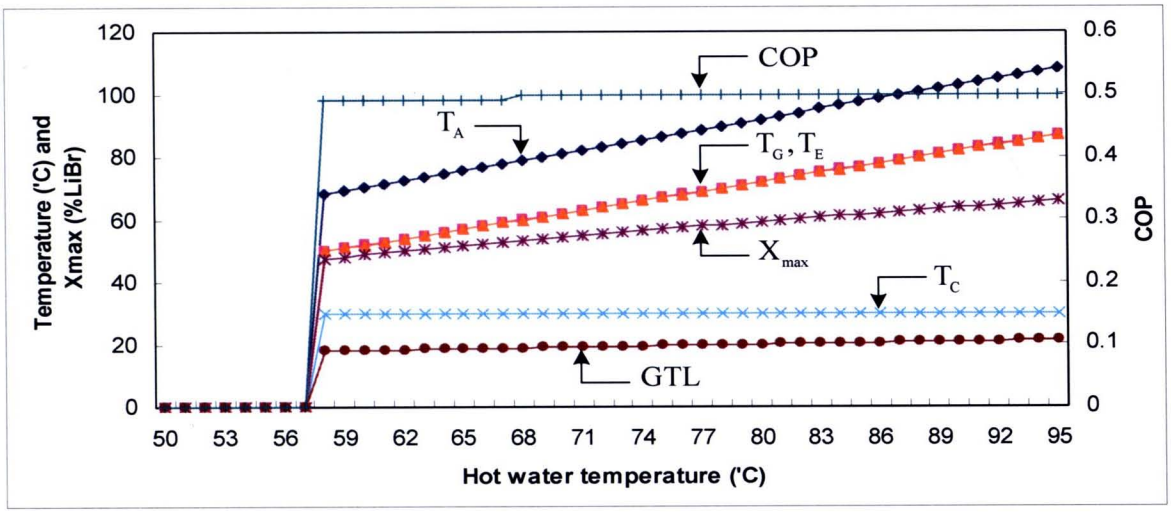

Figure 3.7 Temperatures, LiBr concentrations and COP of the AHT components at various supplied hot water temperatures.

3.5.2 Comparison of the Thermal Performance of the Solar-AHT and the Solar-CAHT with Single-Stage VCHP

In this section, the performance of the solar-AHT is considered and compared with those of the solar-CAHT. Both systems get heat from a set of flat-plate solar collectors each in parallel connection. The solar collector characteristics, $F_R(\tau\alpha)$ and F_RU_L, of flat-plate solar collectors are 0.802 and 10.37 W/m^2·K (Sanguantrakarnkul, 2006).

For the simulation, the solar radiation (I_T) and the ambient temperature (T_{amb}) of Chiang Mai, Thailand were taken and April, the hottest month, was selected for the calculation. It could be noted that the AHT could be operated when the hot water temperature from the solar water heating system was around 58 °C then the minimum units of solar collectors for supplying heat to the AHT was found to be 35 units. The system could operate continuously about 5 h/d. The solar-AHT supplied heat about 20 kW at the evaporator and the generator and generated upgraded heat about 10 kW at a higher temperature level at the AHT absorber.

Figure 3.8 shows temperatures of the solar-AHT components for 35 units of the flat-plate solar collector during the average day of April. The AHT could operate at around 11 a.m. when the hot water temperature was around 58 °C. It could be seen that the absorption system could generate heat at the absorber which was over 70 °C.

T_C was nearly constant while T_G, T_E and T_A varied with the hot water temperature from the solar water heating system. Figure 3.9 shows the heat rates at all components of the system.

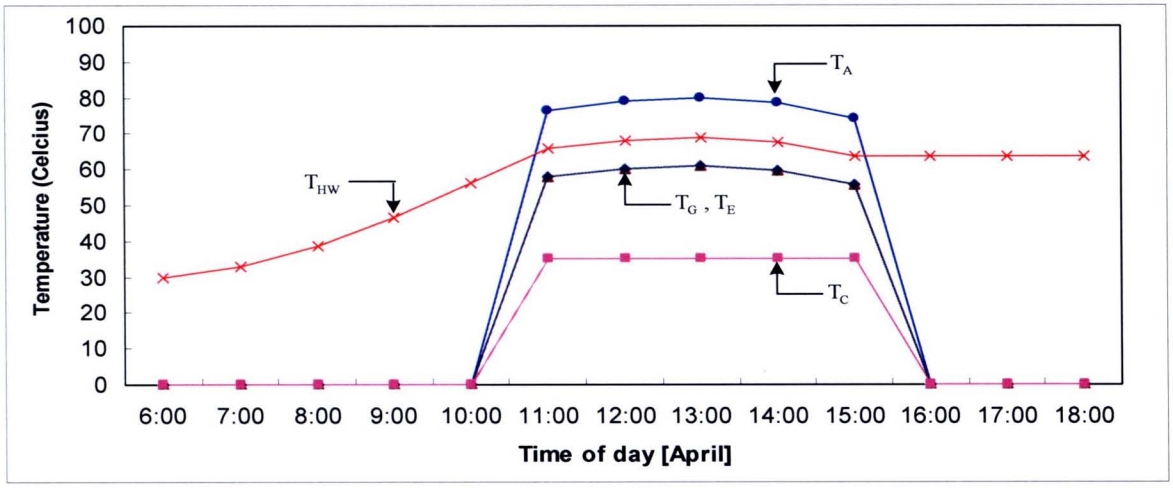

Figure 3.8 Temperatures of the solar-AHT components for 35 units (area 2 m^2/unit) of flat-plat solar collectors during time of the average day of April.

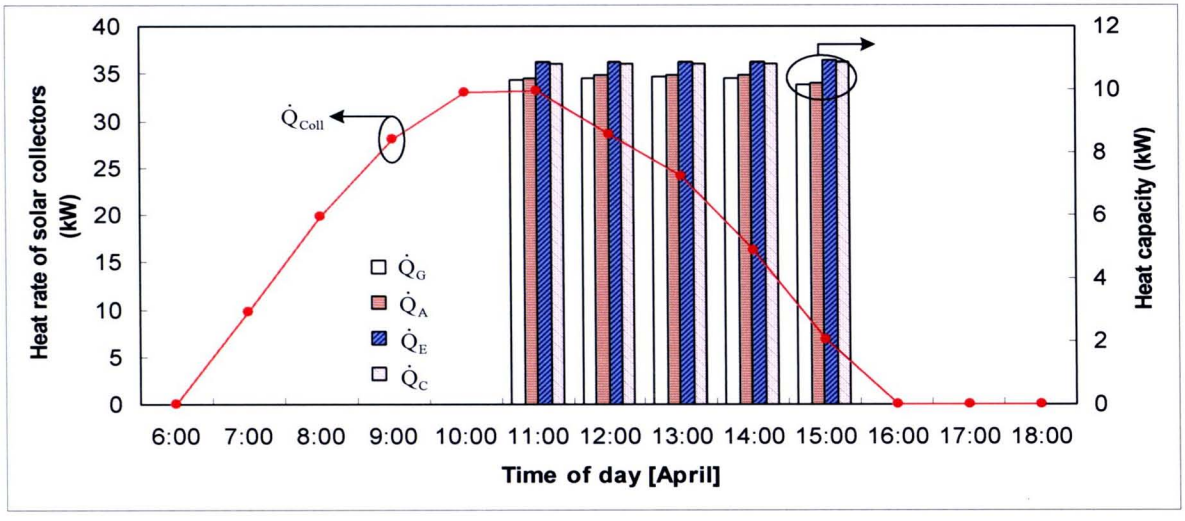

Figure 3.9 Heat rates at the solar-AHT components for 35 units (area 2 m^2/unit) of flat-plat solar collectors during time of the average day of April.

Figure 3.10 shows the temperature profiles of the solar-CAHT components of flat-plate solar collectors. It could be seen that T_E and T_A were nearly constant while T_G varied with T_{HW} from the solar water heating system. The heat rates from solar heat and the heating capacities of the AHT components are shown in Figure 3.11. It could be noted that the system required the flat-plate solar collectors only 18 units.

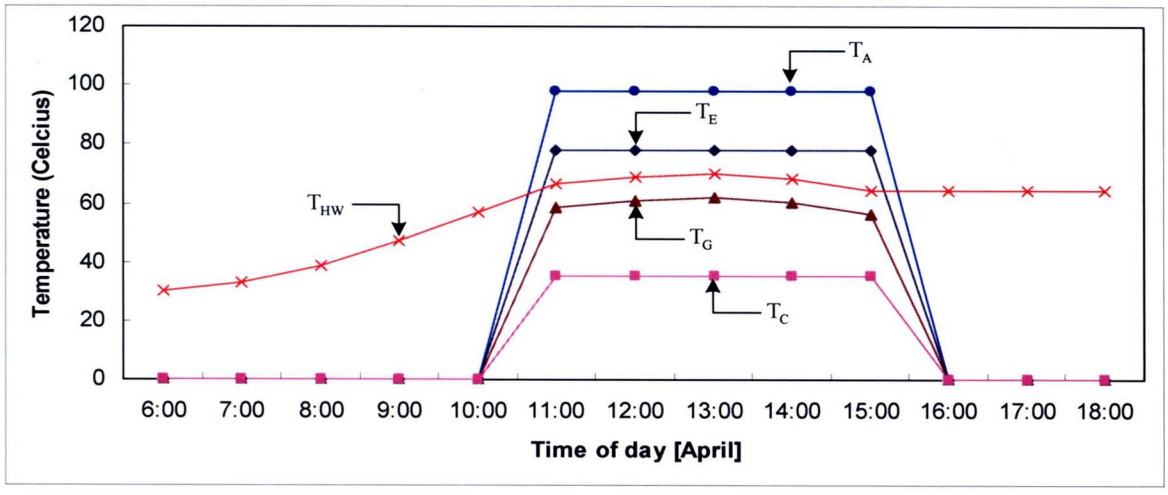

Figure 3.10 Temperatures of the solar-CAHT components for 18 units (area 2 m^2/unit) of flat-plat solar collectors during time of the average day of April.

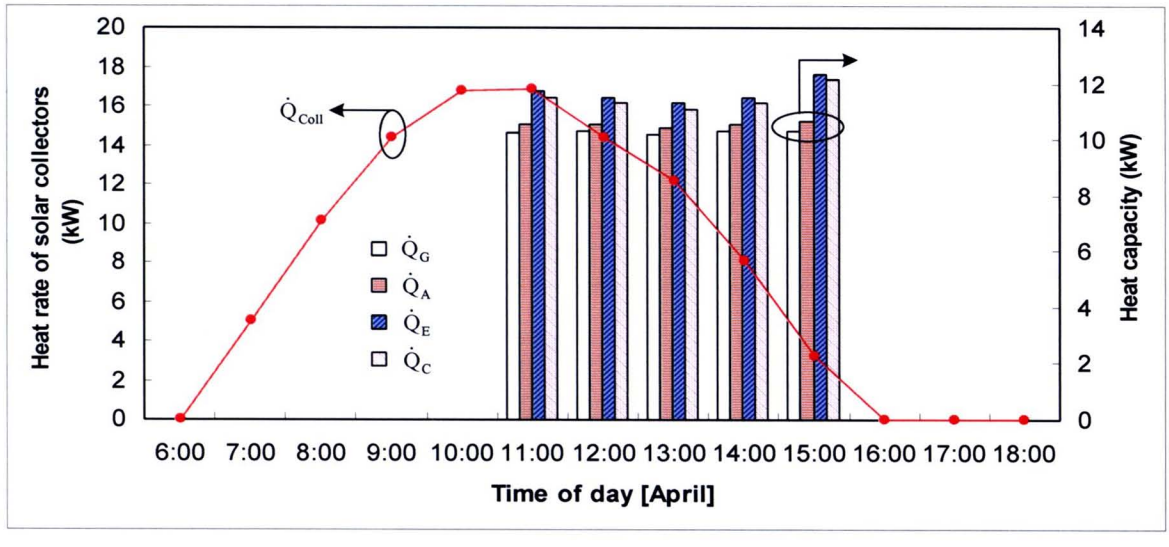

Figure 3.11 Heat rates of the solar-CAHT components for 18 units (area 2 m^2/unit) of flat-plat solar collectors during time of the average day of April.

Figure 3.12 shows the overall COP of the normal solar-AHT and the solar-CAHT with flat-plate solar collectors during time of the average day of April. It could be found that the overall COP of the solar-CAHT having flat-plate solar collectors increased around 60% which was 0.77 compared with 0.49 of the solar-AHT with flat-plate solar collectors. The number of flat-plate solar collectors was 18 units compared with that of the solar-AHT which was 35 units.

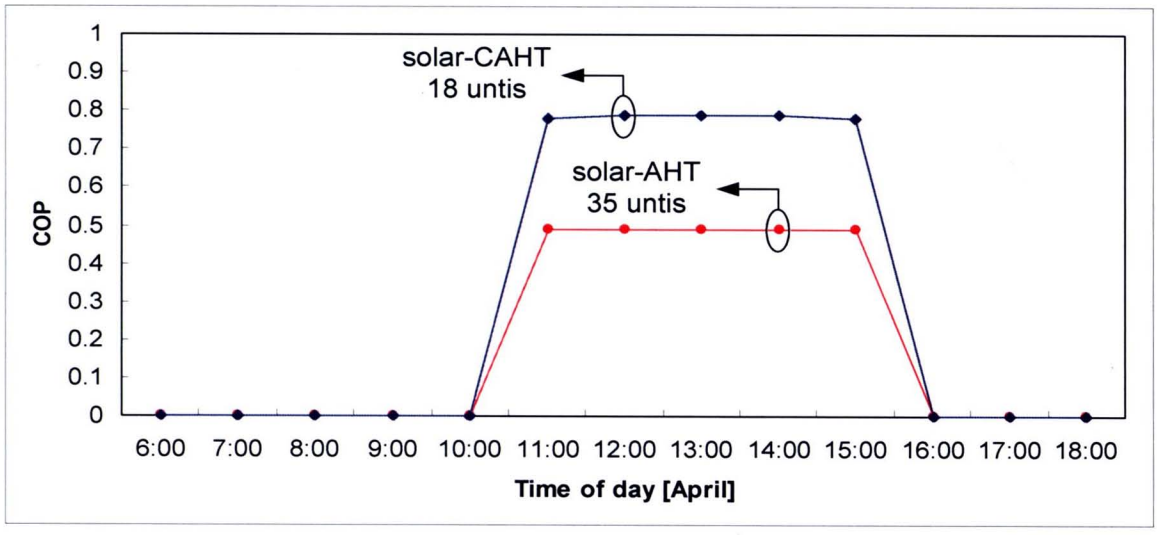

Figure 3.12 Comparison of the overall COP of the solar-AHT and the solar-CAHT on I_T during time of the average day of April.

3.5.3 Comparison of the Thermal Performance of the Solar-AHT and the Solar-CAHT with Two-Stage VCHP

Figure 3.13 shows comparisons on the performances of the single-stage and two-stage VCHPs. It could be seen that the latter one could be better COP and the heating capacity.

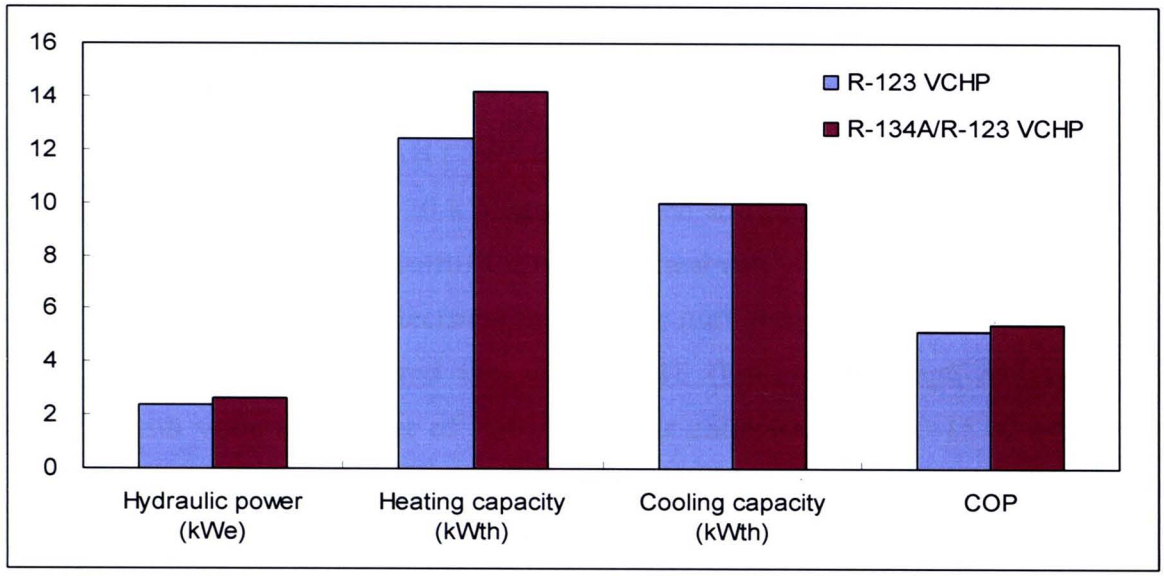

Figure 3.13 Comparison of the thermal performance of the R-123 VCHP and R-134A/R-123 VCHP at T_E 40 °C and T_C 90 °C.

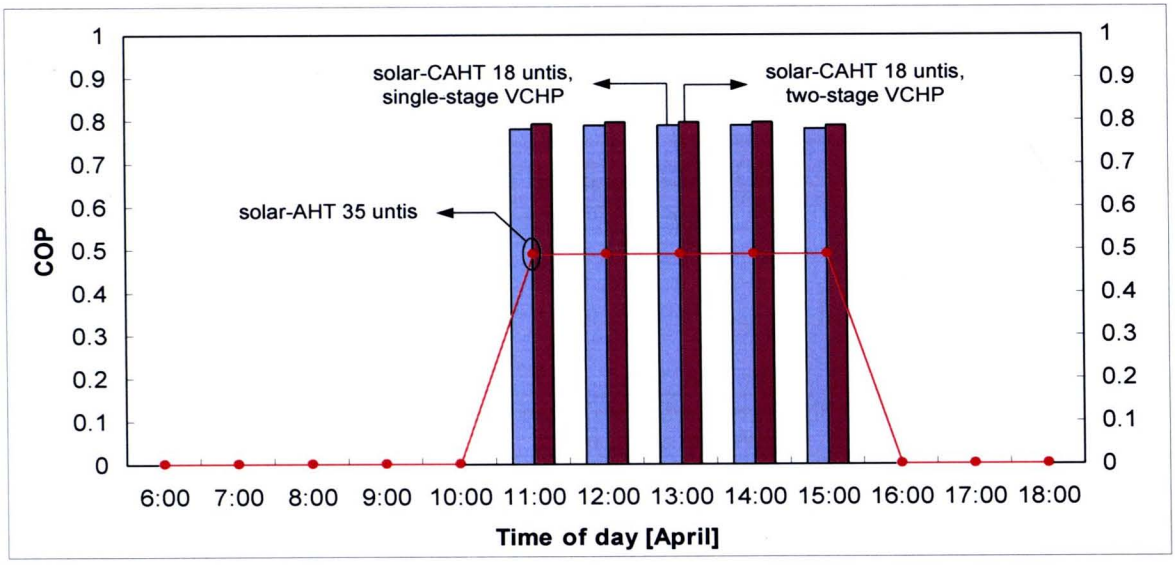

Figure 3.14 Comparison of the overall COP of the solar-AHT and the solar-CAHT of single-stage VCHP and two-stage VCHP on I_T during time of the average day of April.

Figure 3.14 also shows the overall COP of the solar-CAHT with two-satge VCHP during time of the average day of April. It could be seen that the overall COP of the solar-CAHT with the two-stage VCHP gives higher value than that with the single-stage and the normal AHT.

3.5.4 Consumption of Total Electrical Power

Normally, the solar-AHT requires heat at the AHT generator and the AHT evaporator which are around 20 kW and when the solar heat is not high enough then an auxiliary heater is used to fulfill the required heat rate.

Comparison of total electrical heat power (auxiliary heat rate and compression power) for the solar-AHT and the solar-CAHT (both single-stage and two-stage VCHPs) with various number of flat-plate solar collectors at 9.00-15.00 of day are shown in Figure 3.15. It could be seen that the solar- CAHT needs less number of solar collectors compared with the normal solar-AHT. With the VCHP, the CAHT then needs less auxiliary than the normal AHT. However, when the compression power is included, more total electrical power is consumed. The CAHT with two-stage VCHP gives less total electrical power consumption than that with single-stage

VCHP. It could be noted that when the number of solar collectors increases, the power consumption is less due to the less auxiliary power.

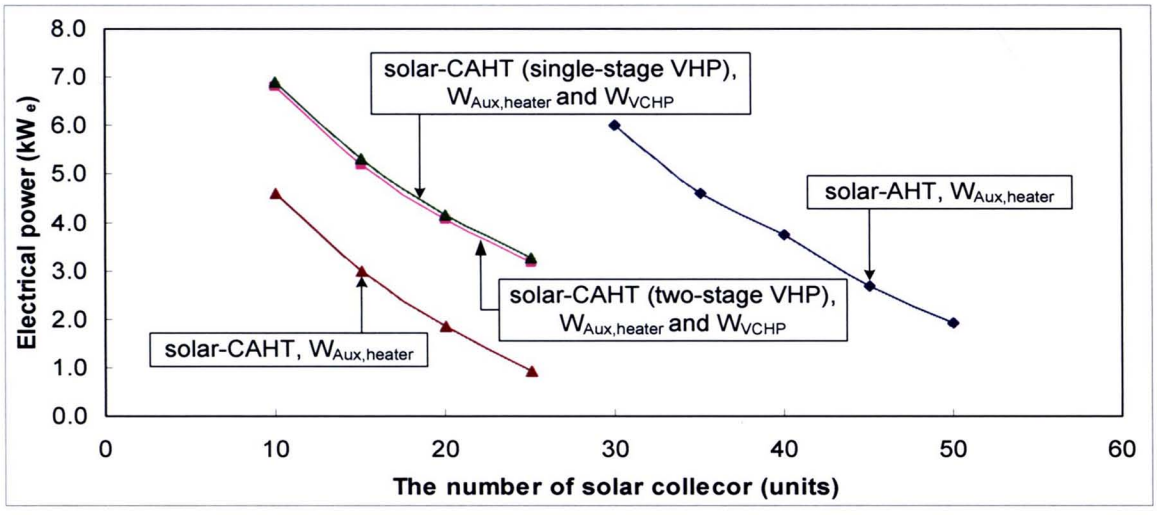

Figure 3.15 Comparison of total electrical power of solar-AHT and solar-CAHT at various number of flat-plate solar collectors at 9.00-15.00 of day for generating heat at absorber 10 kW_{th}.

3.6 Conclusions

From this study, the conclusions are as follows:

1. The overall COP of the solar-CAHT could be increased around 60% which was around 0.8 compared with around 0.5 for the normal solar-AHT.
2. For 10 kW heat rate with the absorber temperature over 80 °C, the number of the solar collectors units of the solar-CAHT could be decreased about 50 % which was 18 units instead of 35 units of the normal solar-AHT.
3. The total electrical power of the solar-CAHT in term of the auxiliary heater and the compression power is lower than that of the solar-AHT which uses only the auxiliary heater. Thus the total COP of the modified unit is higher.
4. The two-stage VCHP is suitable to combine with the AHT compared with the single-stage one because of its high COP.